# AN UPDATED CONCEPTUAL MODEL OF THE TOMPASO GEOTHERMAL FIELD USING NUMERICAL SIMULATION

Ade Lesmana[1], Heru Berian Pratama[1], Ali Ashat[1, 2], Nenny Miryani Saptadji[1] and Fatah Gunawan[3]

[1]Geothermal Master Program, Institut Teknologi Bandung, Jalan Ganesha 10, Bandung

[2]Department of Earth Resources Engineering, Faculty of Engineering, Kyushu University, Fukuoka 819-0395, Japan

[3]PT Pertamina Geothermal Energy, Head Office, Skyline Building 14th Floor, MH Thamrin St. no.9, Central Jakarta

adelesmana21@gmail.com

**Keywords:** *Tompaso, TOUGH2, natural state, conceptual model*

## ABSTRACT

Recent geoscience studies and well data suggest that the Tompaso geothermal field may have two separate reservoirs. The first reservoir is located around the LHD-27 well cluster in the Pinabetengan area and it has supplied 2×20 MWe at units 5 and 6 of the Lahendong power plant since the year 2016. The second prospect is located around the Tempang area, which is associated with the Soputan fault. A new conceptual assessment of the Tompaso area is presented based on a numerical reservoir model which was constructed using the TOUHG2 simulator and the EOS1 equation of state. The reservoir model includes two high-temperature upflows at the base of the model, including one below the Masam Crater and one below the Toraget area. The locations of these upflows were chosen based on the appearance of alteration zones. A natural state model was developed based on downhole pressure and temperature data from ten wells. Based on this natural state model, an alternative conceptual model was proposed where the second geothermal prospect area was added. In the first prospect area, the updated conceptual model has the geothermal fluid coming from the upflow zone located below the Masam Crater and then moving north-northeast towards the Kawangkoan area. In the second prospect, the updated conceptual model has geothermal fluid flowing from an upflow zone under the Toraget area and expected moving to the northeast towards the Passo area.

## 1. INTRODUCTION

The Tompaso geothermal field is situated within the Tompaso district, Minahasa Regency, North Sulawesi, or around 60 km from Manado City (Handoko, 2010), as shown in Figure 1. The field is managed by PT Pertamina Geothermal Energy. Exploration of the Tompaso field began in 1982 to meet electricity demand for North Sulawesi. Three exploration wells and five development wells were drilled from 2008 to 2009 to confirm the geology and the size of the geothermal resource. Early exploration suggested a liquid dominated resource with a temperature range of 250°C to 300°C (Gunawan et al., 2015). A resource assessment was performed by Handoko (2010) using a Monte Carlo probabilistic approach to estimate the amount of stored heat in the system. The assessment suggested that the electricity potential for 30 years of operation could be 39 MWe (50% probability). Since the year 2016, the field has provided 2×20 MWe through units 5 and 6 of the Lahendong geothermal power plant (Directorate Geothermal and Center of Mineral, Coal and Geothermal Resources, 2017), with the main production zone located around the LHD-27 well cluster (Handoko, 2010).

The application of numerical simulation to update conceptual models has, for example, been conducted previously by Ashat et al., (2019), Supijo et al., (2018) and Kurniawan et al., (2018). The aim of this study was to develop a numerical natural-state model which can represent the natural reservoir condition of the Tompaso geothermal field. Results of the model could then be used to generate an alternative conceptual model. The natural state model and the conceptual model developed in this study have two separate reservoirs in the Tompaso field.


**Figure 1: Location of the Tompaso geothermal field in North Sulawesi, Indonesia (Google maps, 2019).**

## 2. RESERVOIR CHARACTERISTICS

The permeability structure of the Tompaso field was studied by Sardiyanto et al., (2015). The North Sulawesi province is located at the convergence of three tectonic plates, the Eurasian, Pacific and Australian plate. Due to those conditions, there was double subduction of the Maluku sea which caused the formation of the Minahasa-Sangihe and Halmahera volcanic arcs. The activity of the Minahasa-Sangihe volcanic arc resulted in the formation of two major strike-slip faults named Menado-Kema and Amorang-Malompar that are NW-SE trending. The Tompaso geothermal field is located between those faults (Figure 2).

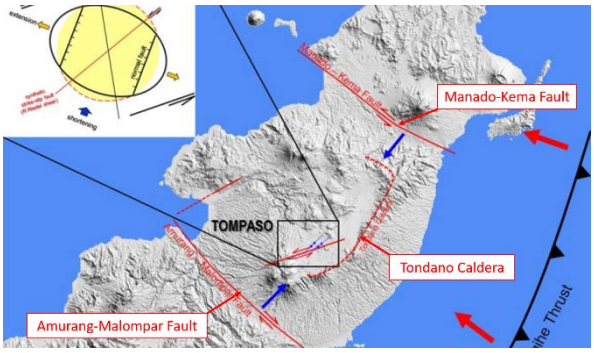


**Figure 2: Geological structure model of Tompaso field (Sardiyanto et al., 2015).**

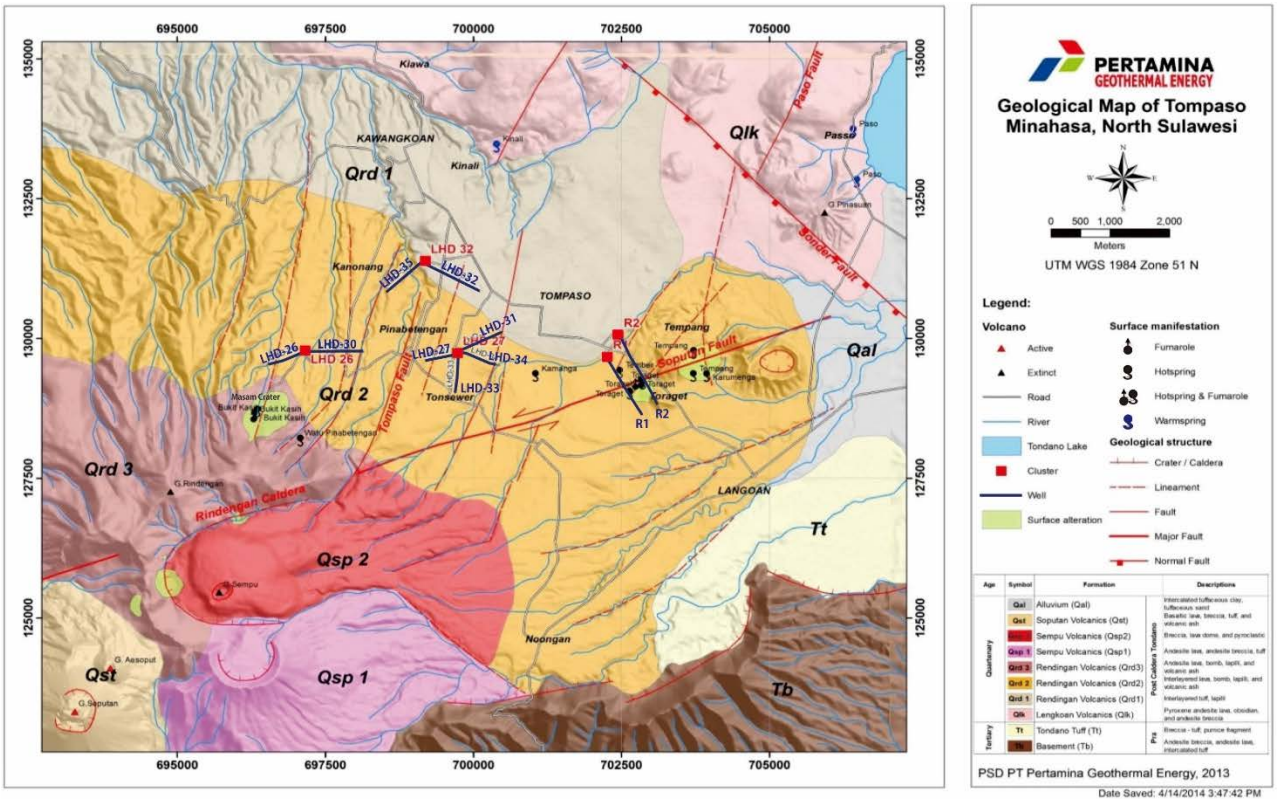


**Figure 3: Geological map of the Tompaso area (modified from Prasetyo et al., 2015; well R1 and R2 azimuth from Gunawan, 2016).**

A structural map of the Tompaso geothermal field is presented in Figure 3. The ENE-SWS trending Soputan Fault is a major strike-slip fault in this area. According to previous study by Sardiyanto et al. (2015), the fault controls fluid movement from the upflow zone in the Riendengan-Sempu area to the Tempang-Toraget area. At the center of the field, the Tompaso Fault is oriented in a NNE-SSW direction, which is a dominant fault orientation for other minor faults in that area. It appears that those faults provide the main permeability in the Tompaso field.

Based on geological evidence, it appears that the magmatic heat source in the area moved over time from the north-east to the south-west, from Mount Lengkoan to Mount Senpu, Mount Rindengan-Maniporok-Aesoput and finally Mount Soputan. The heat source that currently exists is relatively shallow and derived from Mount Soputan (Handoko, 2010).

According to Handoko (2010), the manifestation distribution in the Tompaso field can be divided into four different regions:

- Manifestations in the Tempang – Tompaso – Mount Umeh area are dominated by chloride hot springs, mud pools, acidic hot springs, and steaming ground.
- Manifestations in the Masam Crater – Mount Riendengan area are dominated by fumaroles, solfatara, and hot springs.
- Manifestations in the Kawangkoan – Mount Emung area are dominated by bicarbonate and sulfate hot springs
- Manifestations that appear on the edge of the Tondano lake and Remboken village are dominated by bicarbonate hot springs.

Two prospects with resistivity values of 5–10 ohm-m were inferred based on a magnetotelluric (MT) resistivity study (Handoko, 2010). The main prospect is located under the Masam Crater (Mount Rindengan) and the second prospect is located in the Tompaso-Tempang area. The top of the reservoir in the Masam Crater reservoir is around sea level, and in the Tompaso - Tempang area the top of reservoir is around 500 metres below sea level. The MT study suggested a conductive layer in both prospects with a value between 3–5 ohm-m, which indicates argillic altered rocks (clay) about 750–1000 m thick.

Selected well locations and well tracks in the Tompaso field are also shown in Figure 3. Eight wells which were drilled from the year 2008 to 2009 are distributed in three clusters. They are cluster LHD-26 (wells LHD-26 and LHD-30), cluster LHD-27 (wells LHD-27, LHD-31, LHD-33, and LHD-24) and cluster LHD-32 (wells LHD-32 and LHD-35) (Handoko, 2010). Figures 10 show interpreted natural-state temperature observations in the wells of those clusters. Well LHD-26 was drilled down to -900 masl and showed a conductive temperature profile. The maximum temperature was 250°C. Well LHD-30 had a convective temperature profile at an elevation of -750 to -1000 masl, witht a temperature around 240°C. Typical convective profiles were found at three wells of cluster LHD-27. Their temperatures reached 250°C at elevations of -100 to -500 masl. The other well (LHD-33) had a convective profile at elevations between -950 to -1100 masl. Then at -900 masl the temperature suddenly dropped from 200°C to 125°C. Wells LHD-32 and LHD-35 had comparatively low temperatures.

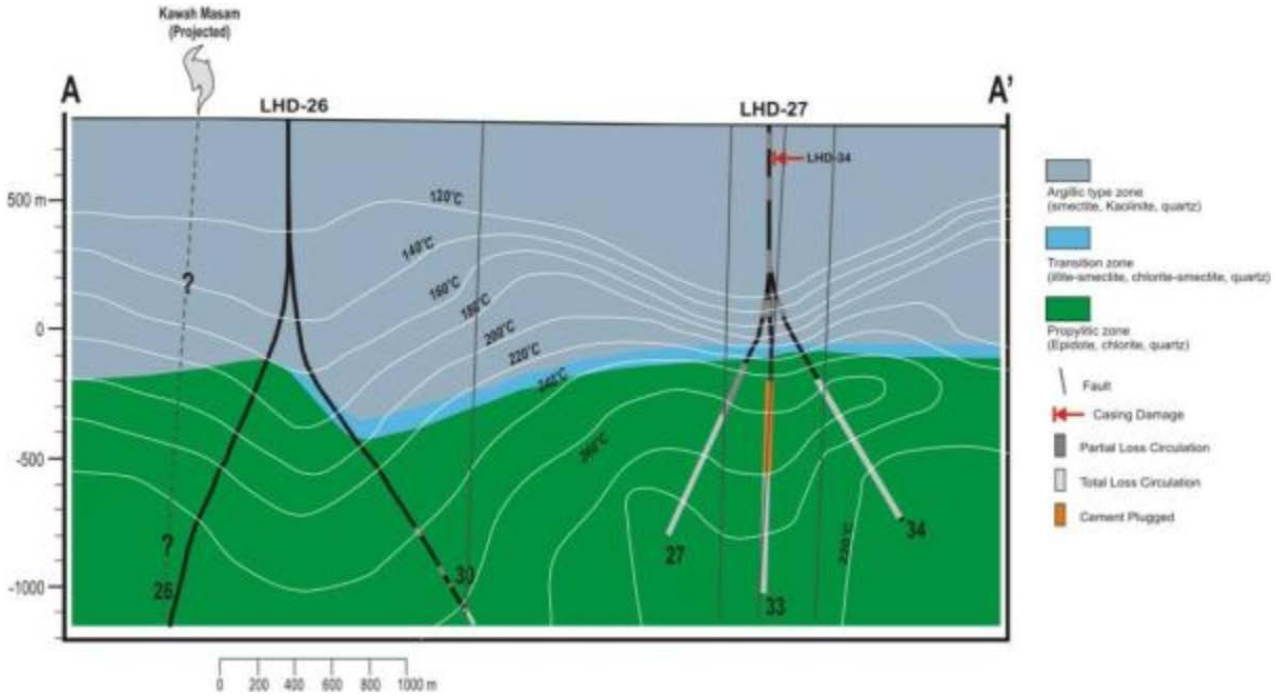


**Figure 4: The Subsurface condition of Tompaso field (Prasetyo and Tri Handoko, (2009) in Handoko (2010)).**

Two additional wells, R1 and R2, were drilled in the Tempang area in 2014 (see Figures 3 and 11). The maximum vertical depth of these wells is about 2600 m. A massive convective zone was found in well R1 at an elevation of -100 to -1940 masl (Gunawan, 2016). The temperature of the convective zone was about 280°C. In well R2 a convective profile was found at elevations between -1500 masl and -1825 masl with its temperature reaching 330°C. Considering the high-temperature profile of both wells, it is possible that there is another heat source or high-temperature inflow around this area. In addition, there is a difference in pressure gradient of well R1 from other well in cluster LHD-26 dan LHD-27, which also indicates that there are two separate reservoir in Tompaso field (see Figure 5).

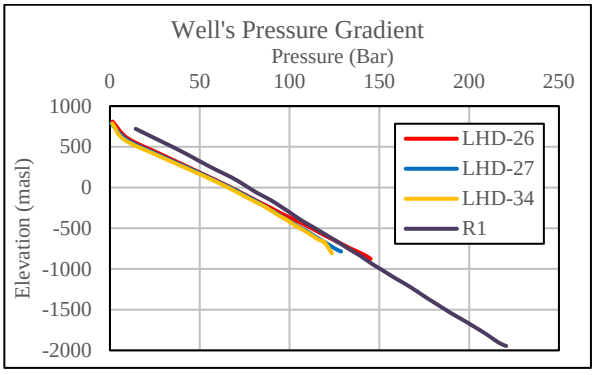


**Figure 5: The difference in pressure gradient of well R1 from other wells in cluster LHD-26 and LHD-27.**

Prior to this study there was no complete conceptual model available for the Tompaso geothermal field. A verticals cross-section showing isothermal temperature profiles is given in Figure 4 for selected wells in the western part of the Tompaso field. The conceptual model has geothermal fluid moving from below the Masam Crater to a shallow depth below cluster LHD-27. The reservoir temperature is 240°C while the top of the reservoir is around -100 masl below cluster LHD-27. It appears that the upflow zone is located under Masam Crater, as indicated by the large number of high-temperature manifestations at the crater.

## 3. NUMERICAL MODEL

### 3.1 The Model Grid

The numerical model of the Tompaso geothermal field was built using the TOUGH2 simulator with the EOS1 equation of state module. The model covers a 39 km$^2$ area and the grid was rotated to align it with the dominant fault trend (Figure 6). The top of the model was constructed to follow the ground topography. The model has 17 horizontal layers extending from 1125 to -2400 masl. The 13 lowest layers have the same thickness of 200 m. One additional 50 m thick layer was added for the atmospheric boundary conditions. All model grid blocks are rectangular and their horizontal dimensions vary from the largest ones being 300×300 m to the smallest ones being 100×100 m in size around wells. The total number of grid blocks was 38,502. Figure 7 shows the 3D model and grid system of the Tompaso field.

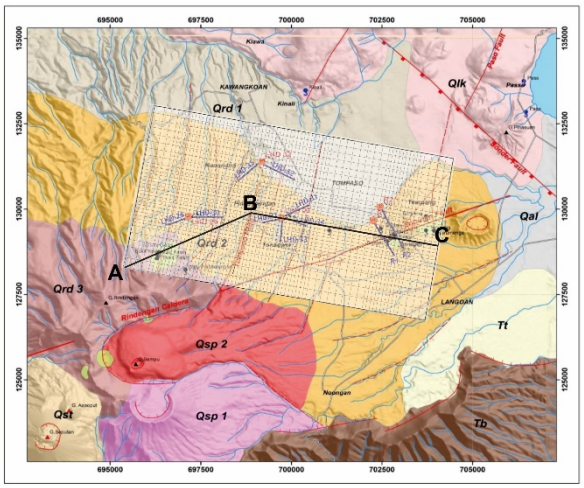


**Figure 6: Top view of the Tompaso field model.**

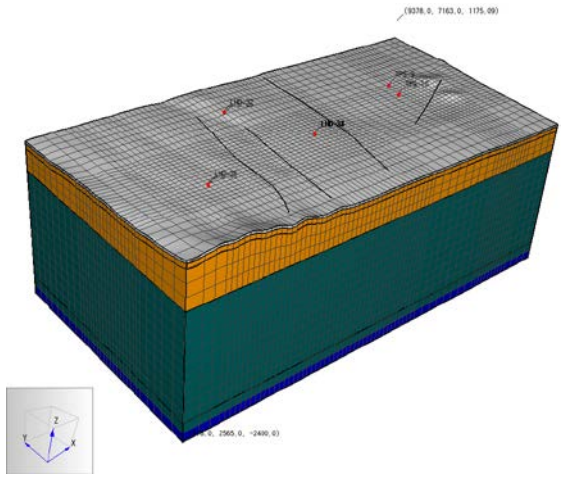

**Figure 7: The 3D model and grid system of the Tompaso field.**

### 3.2 Initial and Boundary Conditions

The top layer was set constant at 1 bar and 25°C to represent atmospheric conditions. The side boundaries are assumed to be no-flow condition. Thus material with permeabilities less than 0.001 mD were assigned for the side boundary.

At the bottom boundary, two high-temperature inflow zones were assigned, while other areas of the bottom boundary were treated as impermeable basement formations. The first inflow was located below the alteration zone of Masam Crater, where 13 blocks had a temperature of 360°C and a pressure of 240 bar as a fixed state. The second inflow zone was located below the alteration zone of the Toraget area, where 20 blocks were used with a constant temperature of 350°C and a pressure of 250 bar. A volume factor of $1\times10^{30}$ also was assigned to both high-temperature inflow area. Several NNE-SSW trending faults were represented in the model, including the Soputan Fault. These faults were referenced when assigning rock types in the model. Figure 8 shows the location of high-temperature inflow (red colour) and assigned faults (black colour) in the 3D model of the Tompaso field. Definition of other color refer to Tabel 1.

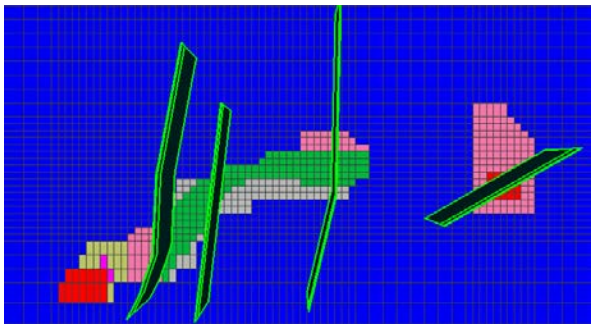

**Figure 8: Bottom boundary and assigned faults.**

### 3.3 Material Properties

Rock types or rock formations were assigned to areas in the model to be representative of rock properties, such as porosity, permeability, density, and specific heat. The most important model parameters in natural state models include rock permeabilities and the bottom boundary conditions (O'Sullivan et al., 2001 and Ashat et al., 2019). The permeability will, in part, control the temperature and pressure distribution by controlling the flow of heat and mass in the model.

Table 1 shows the calibrated permeabilities for each assigned material or rock type. $K_{xy}$ indicates the rock permeability in lateral direction, while $K_z$ shows the permeability in vertical direction, in millidarcy (mD). The permeability of reservoir material ranges between 3 to 100 mD. The rock characteristics curve, relative permeability, uses Corey's curve and has been assigned to all rock material.

Other material properties were uniform across the model (e.g., rock density and specific heat were set uniformly as 2600 kg/m$^3$ and 1000 J/(kg·K). The material distribution of the Tompaso 3D model in proposed conceptual model slicing is shown in Figure 9.

**Tabel 1: Material properties.**

| Material | $K_{xy}$ (mD) | $K_z$ (mD) |
|---|---|---|
| BOND | 0.0001 | 0.0001 |
| BASE | 0.01 | 0.01 |
| ATM | 100 | 100 |
| CAPRK | 0.001 | 0.001 |
| HEAT | 100 | 100 |
| RES1 | 6 | 3 |
| RES2 | 10 | 5 |
| RES3 | 80 | 40 |
| RES4 | 60 | 30 |
| RES5 | 100 | 50 |
| RES6 | 100 | 100 |
| IMPR1 | 0.001 | 0.001 |
| IMPR2 | 0.0001 | 0.0001 |

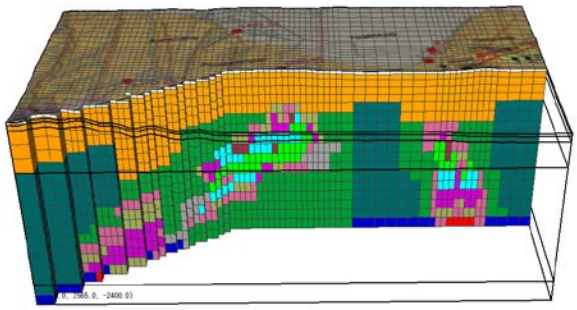

**Figure 9: Material or rock-type distribution.**

## 4. MODEL VALIDATION

Natural-state simulations were carried out by running the model up to a large simulation time to reach a steady-state condition. The final calibrated natural-state model was found by adjusting model permeabilities until the model gave a reasonable match to downhole pressure and temperature observations.

### 4.1 Pressure and Temperature Matching

The simualted pressures and temperatures given by the calibrated model were validated using observations from eight wells around the Pinabetengan area (the LHD wells) and two wells in the Tempang area (wells R1 and R2). However, only seven wells were thought to penetrate the reservoir zone according to pressure and temperature downhole logging data. Wells LHD-32 and LHD-35 did not reach the reservoir zone while the logging data of well LHD-33 appeared to be unreliable since it's temperature decrease lower than normal gradient temperature. Thus those three wells were not considered in the validation step. Figures 10 and 11 compare observed pressures and temperatures with values given by the calibrated model.

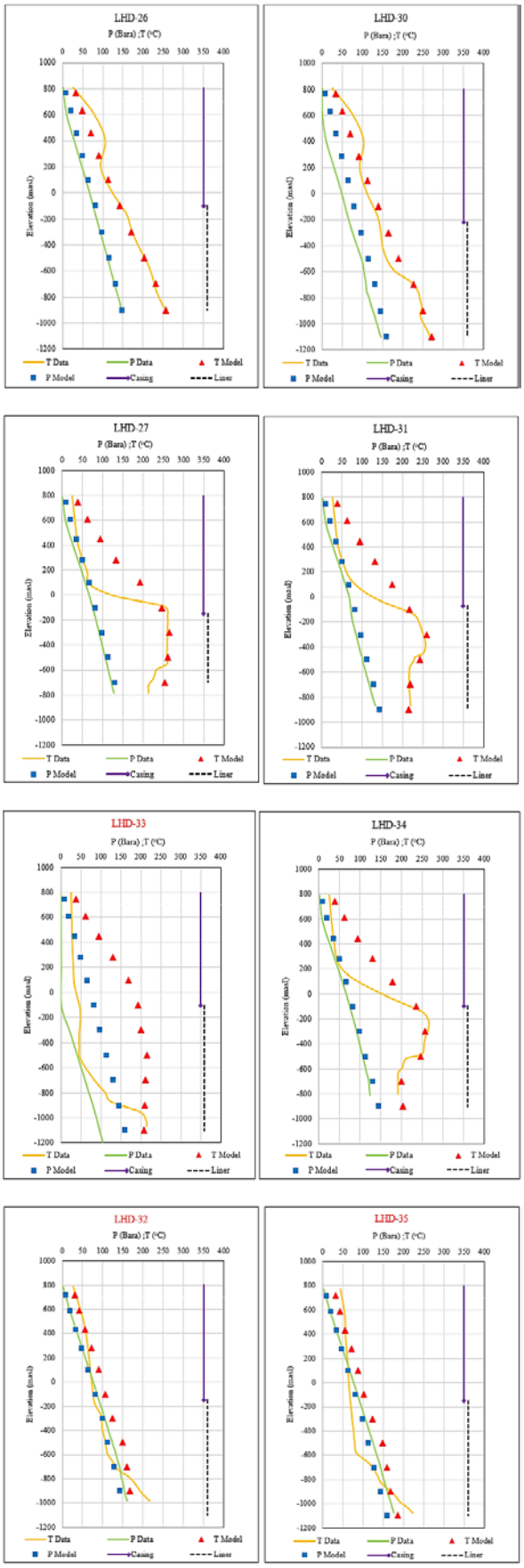


**Figure 10: Pressure and temperature matching results for cluster LHD-26, LHD-27 and LHD-32.**

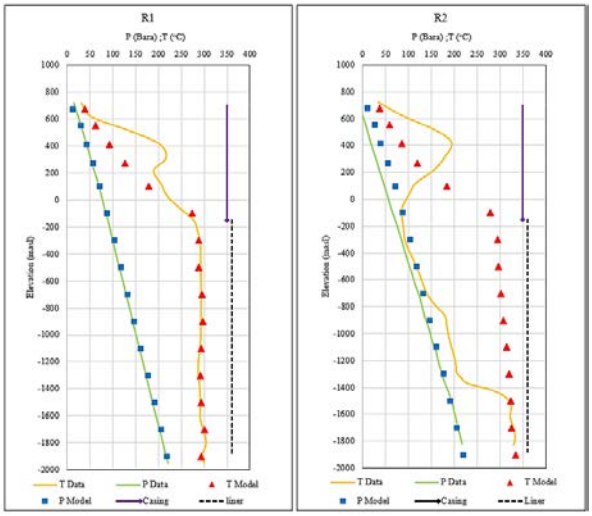


**Figure 11: Pressure and temperature matching results for cluster R1 and R2.**

Figure 12 and 13 shows overall pressure and temperature matching from 7 wells, which were evaluated at liner section only. Data gathered on 45° line indicated a proper matching was achieved. Regarding the significant temperature drop at elevation -1400 masl of R2 well, there is no information to explain this condition. However, since the distance between well R1 and R2 less that 300 m, it was assumed that both wells penetrate the same formation. Then the model's temperature profile of both well's become similar.According to Seyedrahimi-Niaraq et al. (2019), the result of pressure and temperature matching can be evaluated using a root-mean-square-error (RMSE) measure by using the following formula:

$$RMSE = \sqrt{\frac{1}{N}\sum_{i=1}^{N}(X_{Data,i} - X_{Model,i})^2} \quad (1)$$

Here N is the number of observations, $X_{Data,i}$ is the its observation and $X_{Model,i}$ is its corresponding simulated value. Applying the RMSE method separately to each validation well, the RMSE for temperature matching ranged from 4.1 to 20.2°C for temperature observations and from 1.2 to 18 bar for pressure observations (Figure 14).

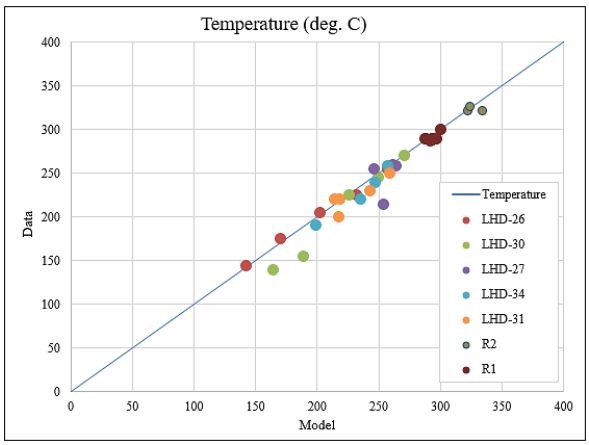


**Figure 12: Comparison of well's temperature data with simulation result for natural state model.**

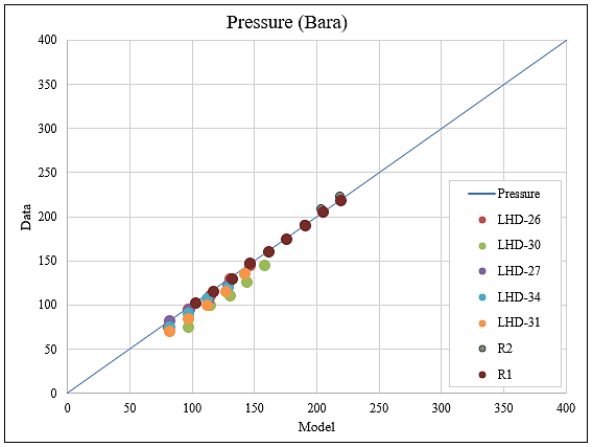


**Figure 13: Comparison of well's pressure data with simulation result for natural state model.**

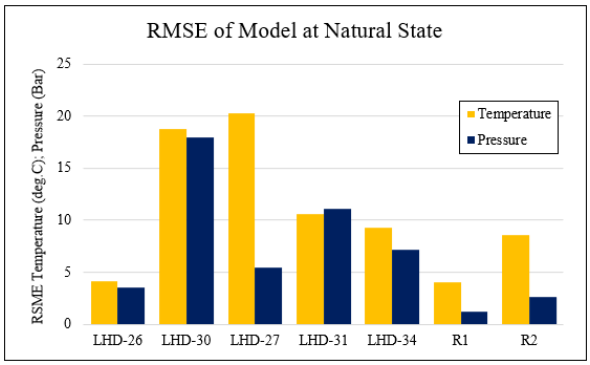


**Figure 14: RMSE of the model at natural state conditions.**

### 4.2 Heat and Mass Flow Directions

Figure 15 shows 3D isothermal profiles and heat flow directions for the calibrated model, while the mass flow directions are shown in Figure 16. The heat and fluid comes from beneath the Masam Crater and the Toraget alteration zone. The appearance of fumarole indicates that both areas include upflow zones of the Tompaso field (see Figure 3). From the Masam Crater, the heat and fluid moves to the east and up to a shallower depth where the Tompaso fault is located. The high-temperature region ends around cluster LHD-27 and forms a "tongue" shape. This result is consistent with the temperature profiles at wells LHD-27, LHD-31, and LHD-34. The appearance of bicarbonate warm springs in the Kawangkoan area to the north is estimated to be caused by an outflow area of fluid flowing from underneath the Masam Crater (Figure 3).

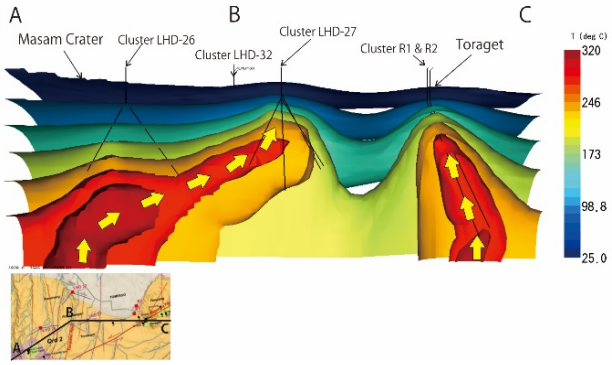


**Figure 15: Temperature isotherms and heat flow vectors for the calibrated model.**

On the other hand, the heat and fluid which comes from beneath the Toraget area is shown in the model to move relatively straight up due to the Soputan Fault. At the surface of this area, there is an abundance of thermal manifestations. The appearance of bicarbonate warm springs on the edge of the Tondano lake in the Passo area suggests an outflow zone for this second prospect (Figure 3). There was no indication of a steam zone in the model which is consistent with downhole logging data. Based on this, the reservoir of the Tompaso field can be categorized as a single-phase liquid system.

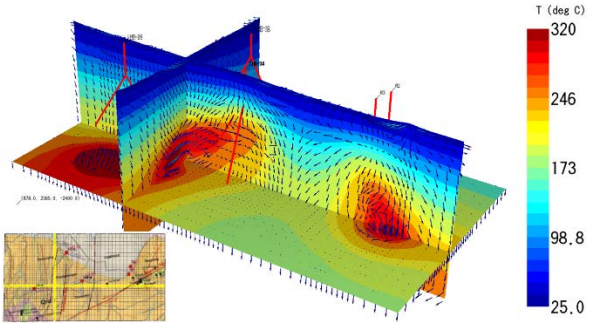


**Figure 16: Fluid flow direction in the model.**

## 5. AN UPDATED CONCEPTUAL MODEL

We used the calibrated 3D numerical model to create an updated conceptual model of the Tompaso geothermal field (Figure 17). For the location of the A-B-C model slice used in Figure 16 refer to Figure 6.

Based on the interpretation of geophysical studies and downhole well data, there are appear to be two separate reservoirs in the Tompaso area. The first prospect is associated with the Masam Crater. The heat is estimated to come from beneath the alteration zone of the Masam Crater. The top of the reservoir in this area is estimated to be at an elevation of -700 to -800 masl. The reservoir extends to the north-east towards the Pinabetengan area where the LHD-27 well cluster is located. In that area, the top of the reservoir is found at a shallower depth at an elevation of about -100 masl. The temperature of the reservoir is around 250 to 270°C. The caprock thickness varies from 750 to 1000 m. Between the reservoir and caprock, there is a 100 m thick transition zone . The upflow zone is located below the Masam Crater while the outflow zone is estimated to be at the Kawangkoan area towards the north side.

The second prospect is located in the Tempang area which is associated with the Soputan Fault. The heat comes from beneath the alteration zone of the Toraget area. In the model, the top of the reservoir is set at an elevation of -200 masl and the temperature of the reservoir ranges between 290 and 320°C. The caprock thickness is estimated to be around 1000 m. The upflow zone is located in the Toraget area while the outflow zone is estimated to be at the edge of the Tondano lake in the Passo area.

The typical temperature profile of well LHD-31 and LHD-34 indicates that both these wells are located at the edge of the reservoir. It appears that the fault which is located between cluster LHD-27 and well R1 in the Tompaso area seperates the two prospects from each other. Because the well's temperature suddenly decrease when the trajectory intersects the fault. According to Gunawan (2016), the recharge area is estimated to be around Tompaso prospect area and possibly from the Tondano Lake.

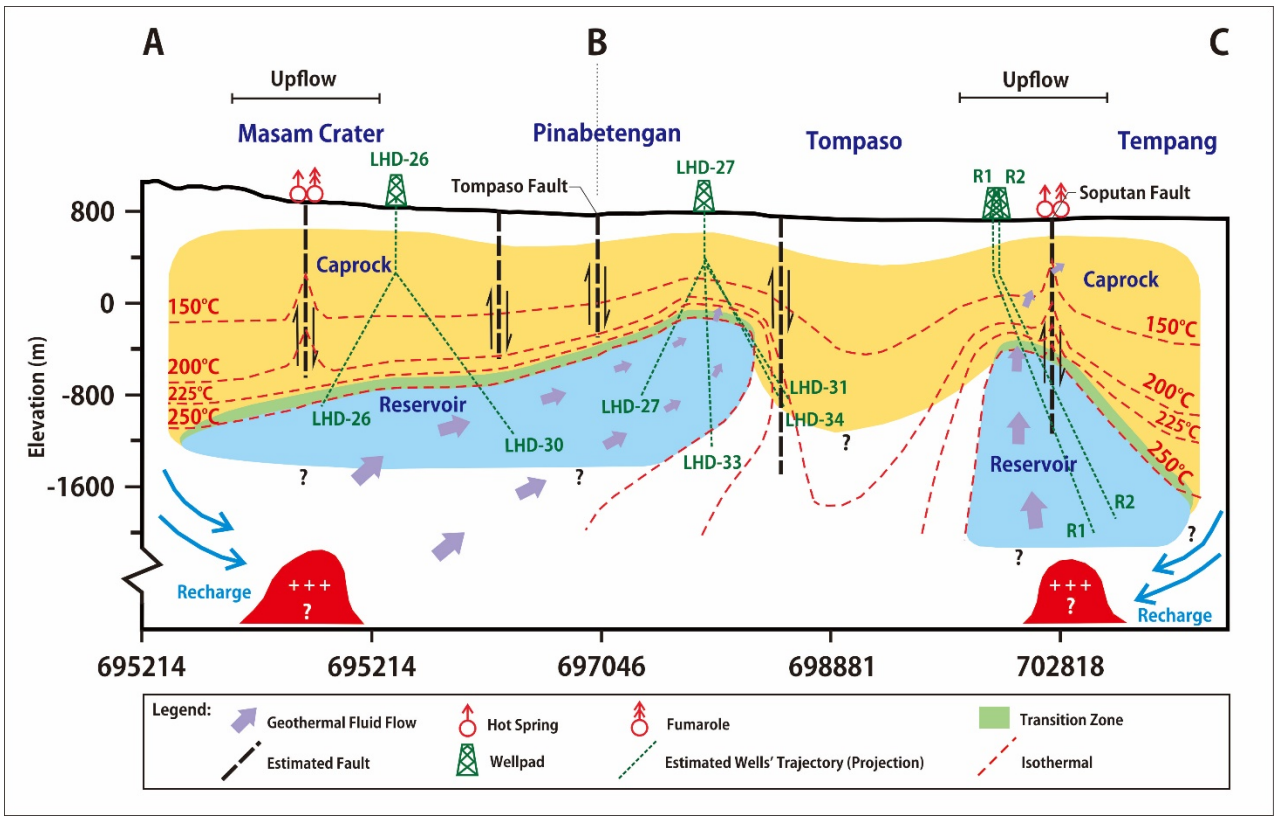


**Figure 17: Proposed conceptual model of Tompaso field based on numerical modelling.**

## 6. CONCLUSIONS

- A numerical model describing the Tompaso geothermal field has been successfully developed and resulted in a good match to natural-state conditions (based on available data and given assumptions).
- For each validation well, the root-mean-square error for the observation matches ranges from 4.1 to 20.2°C for temperature matches and from 1.2 to 18 Bar for pressure matches.
- The model is able to depict the appearance of two separate reservoirs at the Tompaso field. In the model, the first reservoir is shown to be located around the Masam Crater and the second reservoir is shown to be located in the Tempang-Toraget area.
- An updated conceptual model has been generated based on the numerical model.
- The Tompaso geothermal field can be categorized as a single-phase liquid reservoir and high-temperature.

## 7. RECOMMENDATIONS

Further validation with production data (history matching) will increase the model's accuracy. Considering the high-temperature zone and good permeability in the Tempang-Toraget are, there is a possibility of another productive area in the south of Toraget controlled by the Soputan Fault.

## ACKNOWLEDGMENTS

The author would like to thank his family for their sacrifice and understanding so that this paper could be finished. The author also would like to thank Ridwan, Claudio, Zhafira and Firdaus from Geothermal Master Program ITB for direct assistance that helped to finish this paper.

## REFERENCES

Ashat, A., Pratama, H. B. and Itoi, R.: Updating Conceptual Model of Ciwidey-Patuha Geothermal Using Dynamic Numerical Model, IOP Conf. Ser. Earth Enviromental Sci., (April), doi:10.1088/1755-1315/254/1/012010, (2019).

Directorate Geothermal and Center of Mineral Coal and Geothermal Resources: Potensi Panas Bumi Indonesia, Directorate General of New Energy, Renewable Energy and Energy Conservation, Jakarta., (2017).

Gunawan, F.: Rencana Pengembangan Panas Bumi Lapangan Tompaso Sulawesi Utara dengan Simulasi Reservoir, Institut Teknologi Bandung., (2016).

Gunawan, F., Hastriansyah, G., Prabowo, T. and Zuhro, A. A.: Remedial Work in a Geothermal Well Case Study: Sendangan-3, Tompaso Project, in Proceeding World Geothermal Congress 2015, pp. 1–6, Melbourne, Australia., (2015).

Handoko, B. T.: Resource Assessment of Tompaso Geothermal Field , Indonesia, United Nation Univ. Geotherm. Train. Program. Reports, (30), 647–674, (2010).

Kurniawan, I., Sumartha, A. G. A., Wiradinata, R., Nandaliarasyad, N., Sutopo, Pratama, H. B. and Prabata, T. W.: Updating Conceptual Model of Cisolok-Cisukarame Geothermal Field, West Java, Indonesia, in Proceeding The 6th Indonesia International Geothermal Convention & Exhibition (IIGCE) 2018., (2018).

O'Sullivan, M. J., Pruess, K. and Lippmann, M. J.: State of the Art of Geothermal Reservoir Simulation, Geothermics, 30, 395–429, (2001).

Prasetyo, I. M., Koestono, H. and Thamrin, M. H.: Clay Alteration Study from Wells of Tompaso Geothermal Field, North Sulawesi, Indonesia, in Proceeding World Geothermal Congress 2015, Melbourne, Australia., 2015.

Sardiyanto, Nurseto, S. T., Prasetyo, I. M., Thamrin, M. H. and Kamah, M. Y.: Permeability Control on Tompaso Geothermal Field and Its Relationship to Regional Tectonic Setting, in Proceeding World Geothermal Congress 2015, Melbourne, Australia., (2015).

Seyedrahimi-Niaraq, M., Ardejani, F. D., Noorollahi, Y., Porkhial, S., Itoi, R. and Nasrabadi, S. J.: A Three-dimensional Numerical Model to Simulate Iranian NW Sabalan Geothermal System, Geothermics, 77(August 2018), 42–61, doi:10.1016/j.geothermics.2018.08.009, (2019).

Supijo, M. C., Wahjono, A. D., Lesmana, A., Harahap, A. H., Sutopo, Pratama, H. B. and Prabata, T. W.: Updating Conceptual Model Using Numerical Modelling for Geothermal Green Field Prospect Area in Atadei , East Nusa Tenggara , Indonesia, in Proceeding The 6th Indonesia International Geothermal Convention & Exhibition (IIGCE) 2018., (2018).